1998

A Preliminary Assessment of Wave, Current, and Sediment Interactions on the Louisiana Shoreface Adjacent to the Isles Dernieres

David A. Pepper
Louisiana State University

Gregory W. Stone
Louisiana State University, gagreg@lsu.edu

Ping Wang
Louisiana State University, pwang@usf.edu

Recent Research In Coastal Louisiana:

Natural System Function and Response to Human Influence

A Symposium
1998

Recent Research in Coastal Louisiana: Natural System Function and Response to Human Influence

A symposium convened by the
Louisiana Universities Marine Consortium
February 3-5, 1998
Lafayette, Louisiana

Edited by

Lawrence P. Rozas
John A. Nyman
C. Edward Proffitt
Nancy N. Rabalais
Denise J. Reed
R. Eugene Turner

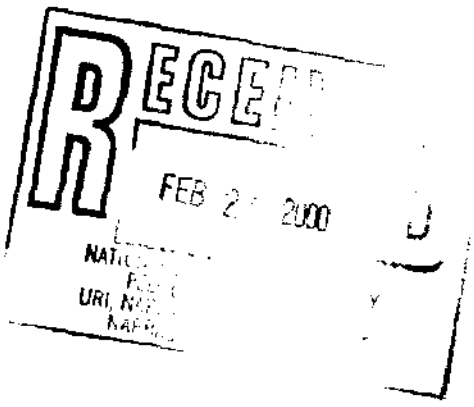

ACKNOWLEDGMENTS

This symposium was funded by generous grants and support from the Louisiana Universities Marine Consortium (LUMCON), Louisiana Sea Grant Program, Coastal Ecology Institute of Louisiana State University, Louisiana Environmental Research Center of McNeese State University, U.S. Environmental Protection Agency, U.S. Geological Survey in Baton Rouge, NOAA Coastal Services Center, Louisiana Department of Natural Resources, LUMCON Foundation, Inc., T. Baker Smith and Sons, Inc., and the Coalition to Restore Coastal Louisiana. The meeting was planned and organized by Denise Reed, Nancy Rabalais, John Day, Andy Nyman, Ed Proffitt, Lawrence Rozas, Gary Shaffer, and Gene Turner. We thank the presenters and attendees for sharing their research, staying on schedule, and allowing stimulating discussion. The following persons assisted tremendously in the preparation of this volume by reviewing the manuscripts presented here: Clark Alexander, Jim Allen, Mahalingam Baskaran, Aaron Bass, Thomas Bianchi, Donald Boesch, Kirk Bundy, Donald Cahoon, Dan Childers, Robert Christen, Robert Costanza, Sherri Cooper, John Dingler, Quay Dortch, Mike Durako, Keith Edwards, Steve Farber, Miriam Fearn, Mark Ford, Jon French, Gary Gaston, Robert Grambling, Courtney Hackney, Ken Heck, Fred Hitzhusen, Clint Jeske, Barb Kleiss, Dwight LeBlanc, Paul Leberg, Terry Logan, Lynn Leonard, Karen Manel, Brent McKee, Thomas Minello, Cynthia Moncrief, Hillory Neckles, William Nuttle, Chris Onuf, Jonathan Pennock, Gary Ray, Harry Roberts, Rickey Ruebsamen, Gary Shaffer, Charles Simenstad, Fred Sklar, Donny Smoak, Thomas Soniat, Marilyn Spalding, Karen Steidinger, Judy Stout, Eric Swenson, Robert Twilley, Ivan Valiela, Milan Vavrek, Shio Wang, James Webb, and Erik Zobrist. We greatly appreciate the efforts of Bonnie Ducote with the Louisiana Sea Grant College Program for her work on the production of this volume.

Published by the Louisiana Sea Grant College Program, a part of the National Sea Grant College Program maintained by the National Oceanic and Atmospheric Administration of the U.S. Department of Commerce. 1999.

Louisiana Sea Grant
Communications Office
Louisiana State University
Baton Rouge, LA 70803-7507
225-388-6449
FAX 225-388-6331
Web site: http://www.laseagrant.org

A Preliminary Assessment of Wave, Current, and Sediment Interaction on the Louisiana Shoreface Adjacent to the Isles Dernieres

DAVID A. PEPPER[1]
Department of Oceanography and Coastal Sciences, Louisiana State University, Baton Rouge, LA 70803, TEL: 225-388-4728; FAX: 225-388-2520; email: dpepper@tiger.lsu.edu

GREGORY W. STONE
Coastal Studies Institute and Department of Oceanography and Coastal Sciences, Louisiana State University, Baton Rouge, LA 70803, TEL: 225-388-6188; FAX: 225-388-2520; email: gagreg@unix1.sncc.lsu.edu

PING WANG
Coastal Studies Institute, Louisiana State University, Baton Rouge, LA 70803, TEL: 225-388-5330; FAX: 225-388-2520; email: pwang2@unix1.sncc.lsu.edu

[1]Corresponding author

ABSTRACT: The Louisiana coast is generally characterized as a low wave-energy environment where sediment transport is dominated by the influence of the Mississippi and Atchafalaya Rivers. Winter cold fronts, however, generate waves and currents that have a significant impact on a variety of Louisiana's coastal environments, although field data regarding their influence on the inner shelf are extremely sparse. During a 12-d period that included the passage of two cold fronts, waves and near-bed currents were measured on the Louisiana inner-shelf (depth ~ 8 m) using a sophisticated bottom-mounted instrumentation system. Bottom boundary layer parameters were then calculated using wave-current interaction models, and sediment transport was predicted by assuming steady state turbulent diffusion within and above the wave boundary layer.

Results indicate that the second front (Front 2) was the more energetic of the two. A maximum significant wave height of 1.33 m and maximum current speed of 0.21 m s^{-1} occurred during this event. Additionally, mean current-induced shear velocity (2.95 cm s^{-1}) and wave-current shear velocity (4.99 cm s^{-1}) were highest during this event's frontal and prefrontal stages, respectively. During the postfrontal stage, currents were strong and well organized, although combined shear velocities were low as a result of reduced wave height. Predicted sediment transport varied considerably in direction and magnitude throughout the deployment, but was highest (12.7-16.2 mg cm^{-1} s^{-1} toward the southeast) during the prefrontal and frontal stages of Front 2. Fair weather transport was low and to the west. Thus, winter cold fronts are likely an important mechanism for sediment movement on the Louisiana inner shelf, although the associated transport direction and magnitude require further quantification.

From the Symposium *Recent Research in Coastal Louisiana: Natural System Function and Response to Human Influence.* Rozas, L.P., J.A. Nyman, C.E. Proffitt, N.N. Rabalais, D.J. Reed, and R.E. Turner (editors). 1999. Published by Louisiana Sea Grant College Program.

Introduction

The Mississippi and Atchafalaya Rivers introduce vast amounts of sediment into the wetland, estuarine, shoreface, and shelf systems along the northern Gulf of Mexico, particularly along the Louisiana coast (Crout and Hamiter 1979). Although much of this material is deposited locally, a considerable amount of fine material is transported with prevailing currents as suspended sediment plumes and deposited offshore. Not surprisingly, therefore, these fluvially-derived sediments serve as important sources of depositional material on the shoreface and continental shelf (Crout and Hamiter 1979; Adams et al. 1987; Roberts et al. 1987; Wright et al. 1997).

In contrast, the importance of entrainment and transport of inner-shelf bottom sediment by waves and currents along the Louisiana coast is poorly documented and quantified. Entrainment of sediment from the bed requires the combined action of waves and currents to generate a shear velocity (u_*) that exceeds a critical threshold determined predominantly by sediment diameter. Since the northern Gulf of Mexico is generally considered a low-energy environment, sediment transport on the Louisiana inner shelf during fair weather is likely minimal (Wright and Nittrouer 1995; Jaffe et al. 1997; Wright et al. 1997).

The passage of cold fronts, however, is a notable exception to these low-energy, fair-weather conditions. Occurring with a frequency of roughly 30 times yr^{-1}, chiefly between November and April (Roberts et al. 1987), the passage of cold fronts generates important hydrodynamic and sedimentary responses in various coastal environments in Louisiana, including deltaic wetlands (Murray et al. 1993), the chenier plain (Roberts et al. 1987), and barrier islands (Dingler and Reiss 1990; Stone and Wang 1999). Data on inner-shelf bottom boundary layer and seabed responses to frontal passages in this region, however, are sparse. With the exception of Jaffe et al. (1997), who modeled sediment transport using representative values of wave and current parameters rather than direct field measurements, no published data for south-central Louisiana are available.

Our objective is to discuss the results of a 12-d instrumented field deployment that included two cold front passages and two intervening low-energy periods. Waves, near-bottom currents, and bottom boundary layer parameters are quantified and used to predict sediment transport magnitude and direction. The results are significant in a practical sense, given that the inner shelf is an important component of the sedimentary system that includes south-central Louisiana's barrier islands and coastal wetlands, which are currently experiencing extremely high rates of erosion.

Materials and Methods

Water level, wave, current, and seabed elevation data were collected from November 20 to December 1, 1997, at an 8-m deep, sandy-bottomed, site on the Louisiana shoreface (Fig. 1) using a bottom-mounted instrumentation system named WADMAS (Fig. 2). The system included a Fluxgate™ compass, a Paroscientific™ pressure transducer, a Digisonics™ sonar altimeter, and a vertical array of three bi-axial Marsh-McBirney™ electromagnetic current meters (at elevations of 20, 67, and 120 cm above the bed). Sensors were programmed for burst-mode sampling; specifically, the pressure sensor and current meters sampled for 8.2 min h^{-1} at a frequency of 4 Hz, while the compass and altimeter recorded one measurement every 30 min.Samples of bottom sediment were obtained using a grab-sampler, and later were dry-sieved to determine mean grain size. Additionally, hourly meteorological data from C-MAN Station GDIL1 (Grand Isle) and daily weather maps from the Southern Regional Climate Center in Baton Rouge, Louisiana were acquired.

Meteorological events were analyzed using a qualitative approach in which each event was subdivided into four stages on the basis of changes in wind velocity. Stages included fair weather, and three frontal stages: pre-frontal, frontal, and post-frontal. The threshold established for wind speed associated with pre- and post-frontal conditions was the mean value for the study period plus one standard deviation. The beginning of the pre-frontal

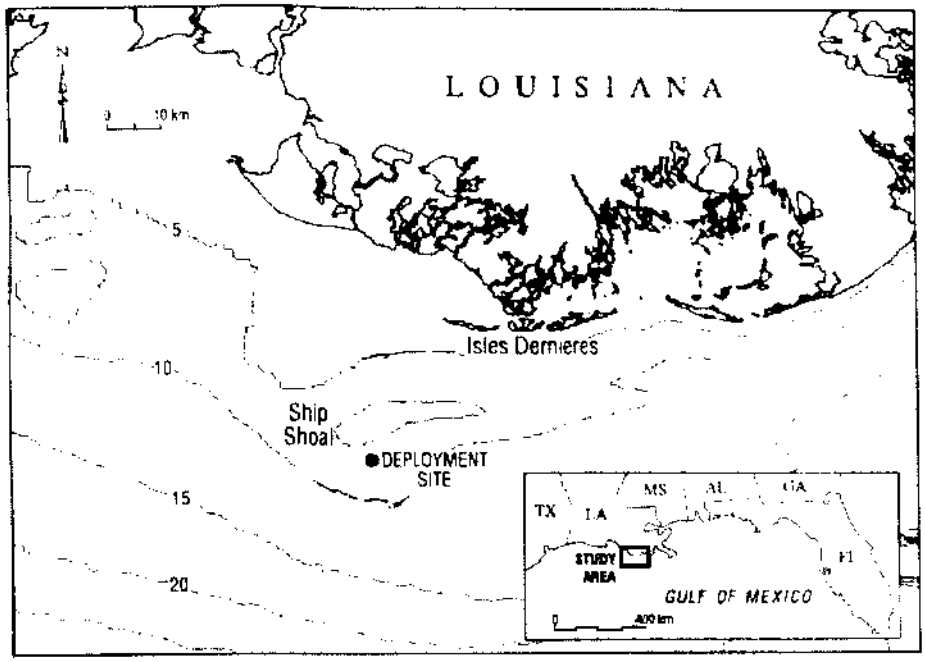

Fig. 1. The Study Area. Instrument was located at 28°50.68′N, 91°07.52′W. Depth contours are in meters.

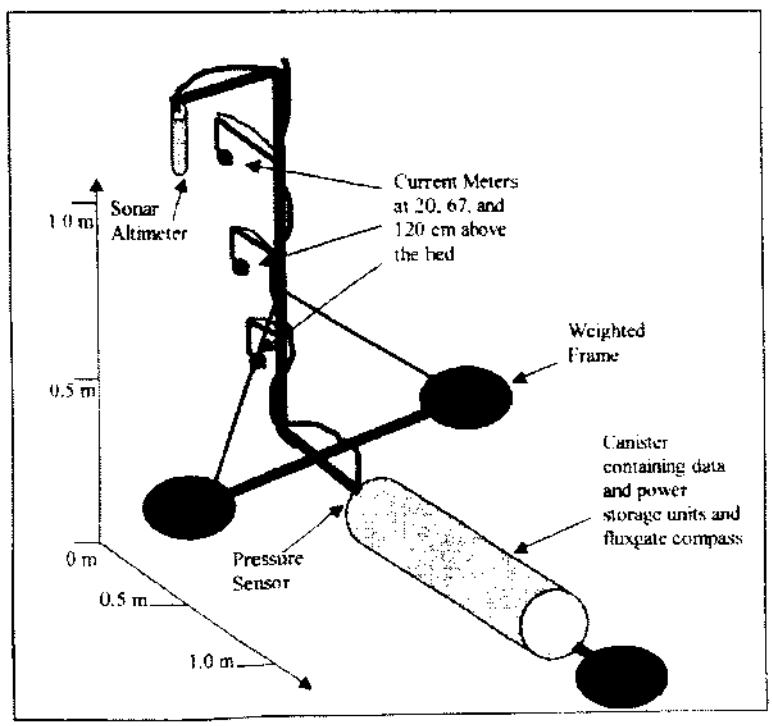

Fig. 2. Schematic diagram of the WADMAS instrumentation system.

phase of the storm was identified as the hour when the wind exceeded this threshold and blew from the south (i.e. between 90° and 270°, measured clockwise). The frontal phase encompassed the period when winds were variable in direction and less than the threshold speed. The post-frontal phase was defined as the interval during which the wind blew from a direction between 270° and 90° at a speed exceeding the threshold. All other wind conditions were considered fair weather.

Significant wave height (H_s), peak wave period (T_p), and mean wave direction (θ_w) were calculated from the pressure and current-meter data using cross-spectral analysis, with horizontal-, and pressure-attenuation correction factors applied to compensate for signal decay with depth (Earle et al. 1995). Current-velocity profiles were generated using the log-profile method, which involves log-linear regression of the burst-averaged current meter velocities (Drake and Cacchione 1992). Two conditions were assumed necessary for a profile to be considered logarithmic in a statistically significant sense: first, a correlation coefficient (r^2) > 0.994 (Drake and Cacchione 1992); and second, a mean directional variation between current meters < 30°. Hourly measurements that were not logarithmic were excluded from the analysis. Current-induced shear velocity (u_{*c}) and apparent bottom-roughness length for all logarithmic profiles were calculated using the von Karman-Prandtl equation:

$$u(z) = u_{*c}/\kappa \ \ln(z/z_{0k}) \qquad (1)$$

where u(z) is the horizontal velocity at height z above the bed, and κ is von Karman's constant (0.4). Once the sediment concentration in the water column had been predicted (discussed later in this section), the shear velocity calculations were iteratively modified to account for the possible effects of suspended sediment induced stratification. To do so, the buoyancy parameter (Z/L) employed in the model introduced by Glenn and Grant (1987) was used.

The Grant-Madsen (1979, 1986) model was used to account for the combined influence of waves and currents. According to the model, a wave boundary layer (wbl) of thickness (δ^*_w) develops during wave activity, and the velocity profile is defined separately within and above this layer as:

$$u_c = \frac{u_{*c}}{\kappa}\left(\frac{u_{*c}}{u_{*cw}}\right)\ln\frac{z}{z_{0l}}, \qquad z \le \delta_w$$
$$u_c = \frac{u_{*c}}{\kappa}\ln\frac{z}{z_{0c}}, \qquad z \ge \delta_w \qquad (2)$$

where u_{*c} and u_{*cw} are the current and combined wave-current-induced shear velocities, respectively, z is the height above the bottom, z_0 is the roughness produced by the sand grains (=D/30, where D is the mean grain diameter), and z_{0c} is the apparent bottom roughness experienced by the current above the wave boundary layer. z_{0c} was used because the current experiences drag due to the combined influences of physical elements (grain roughness and bed forms) as well as non-linear interaction with the wave boundary and mobile bedload layers (Gross et al. 1992).

The assumptions were made that the current-induced shear velocity, u_{*c}, acts in the same direction as the mean current, and that the direction of u_{*cw} oscillates during the course of the wave cycle. As such, when the wave orbital velocity is at a minimum (near zero), the direction of u_{*cw} is the same as that of the current; when it is at its maximum, its direction (φ_{max}) is between the wave and current directions, given by [modified from Cacchione et al. (1994)]:

$$\varphi_{max} = \arctan\left(\frac{\sin\phi}{\cos\phi + \frac{b}{u}}\right) \qquad (3)$$

Sediment transport was estimated based on the assumption of steady-state, upward, turbulent diffusion of sediment through the water column. First, an entrainment function was defined, based on the Yalin parameter (Ξ):

$$\Xi = [(\rho_s - \rho)gD^3/\rho\nu^2]^{0.5} \qquad (4)$$

where r_s and r are the respective densities of sediment (2.65 g cm^{-3}) and seawater (1.025 g cm^{-3}), D is the grain diameter, and v is the kinematic fluid viscosity (0.013 cm^2 s^{-1}). The critical Shield's criterion (θ_{crit}), and shear stress τ_{crit} were then calculated using:

$$\log\theta_{crit} = 0.041(\log^{\Xi})^2 - 0.356\log^{\Xi} - 0.977 \quad (5)$$

and $$\tau_{crit} = \theta_{crit}(\rho_s - \rho)gD \quad (6)$$

Normalized excess shear stress (S') was then defined as:

$$S = \left(\frac{\tau - \tau_{crit}}{\tau_{crit}}\right) \quad (7)$$

where t is the observed shear stress. This was then used to define the "near-bed" sediment concentration ($C(z_a)$):

$$C(z_a) = C_{bed}\frac{\gamma_0 S}{1 + \gamma_0 S} \quad (8)$$

where C_{bed} is the sediment concentration in the bed (0.65) and γ_0 is an empirical constant with a value of 0.002. Suspended sediment concentrations were assumed to take the form of Rouse profiles, defined by:

$$C(z) = C(z_a)\left(\frac{z}{z_a}\right)^{-\alpha}, \text{ where } \alpha = \frac{\gamma w_s}{\kappa u_*} \quad (9)$$

γ is the ratio of the eddy diffusivity of sediment to that of momentum (~1), and w_s is the particle fall velocity.

Finally, burst-averaged sediment transport (Q) was calculated by integrating the velocity and sediment concentration profiles within, and above, the wave boundary layer such that:

$$Q = \frac{1}{t}\int_{z=\delta_w}^{z=\eta}\int_0^t uC\,dzdt \quad \text{for} \quad z > \delta_w$$
$$Q = \frac{1}{t}\int_{z=z_0}^{z=\delta_w}\int_0^t uC\,dzdt \quad \text{for} \quad z < \delta_w \quad (10)$$

where η is the sea surface elevation, and u is the current velocity.

Results and Discussion

Meteorological Conditions

Meteorological data indicated that the study period could be subdivided into two intervals of fair weather and two cold fronts (hereafter, Front 1 and Front 2). The fair weather phases lasted from 19:00 UTM on November 18 (prior to the deployment) to 18:00 UTM on November 21, and from 03:00 UTM on November 25 until 18:00 UTM on November 28. The fair weather phases were characterized by light (1.3-6.6 m s^{-1}) southerly or easterly winds; whereas both frontal passages were characterized by a sequence of strong southerly winds, followed by light and variable winds, and finally by strong northerly winds (Table 1 and Fig.3). Frontal passages differed from each other in several respects. Strongest winds during the pre- and post-frontal phases were from the south and northeast (respectively) in the case of Front 1 and from the southeast and northwest during Front 2. Most notably, however, these fronts differed markedly in intensity. Front 2, which had maximum pre-frontal and post-frontal wind velocities of 11.3 and 13.7 m s^{-1} was much more powerful than Front 1. Thus, the discussion will focus primarily on hydrodynamic and sedimentary responses associated with Front 2.

Hydrodynamic Responses

The influence of the frontal passages, particularly Front 2, on the wave field is shown in Table 2 and Fig. 4. During fair weather and during the first frontal passage, significant wave height was generally below 0.6 m. In contrast, during the pre-frontal stage of the Front 2, a maximum significant wave height of 1.34 m was measured. The trend in wave height was, not surprisingly, accompanied by a very similar trend in near-bed orbital velocity, which reached a maximum of 55 cm s^{-1} during the pre-frontal stage of Front 2. Patterns in wave period accompanying the frontal passages were less clear, although the pre-frontal and frontal phases of Front 2 were notable for the presence of comparatively long period waves, and peak period was observed

Table 1. Characteristics of the cold front passages. Note that "direction" follows the meteorological convention, indicating the direction from which the wind was blowing. Key: U_w = mean wind speed. [a] the first fair weather period began prior to the deployment.

Front	Phase	Arrival Time (m/d/h)	Mean U ($m\ s^{-1}$)	Range of U ($m\ s^{-1}$)	Dominant Direction
1	Fair	11/18/19:00 [a]	4.2	2.7 – 6.2	South
	Pre	11/21/18:00	5.6	4.3 – 6.9	South
	Front	11/22/4:00	3.1	1.5 – 4.3	Variable
	Post	11/22/21:00	6.7	2.9 – 9.0	Northeast
2	Fair	11/25/3:00	4.1	1.3 – 6.6	East
	Pre	11/28/18:00	7.0	3.6 – 11.3	Southeast
	Front	11/29/16:00	2.1	0.3 – 3.4	Variable
	Post	11/30/6:00	8.7	5.4 – 13.7	Northwest
ALL	—	—	5.3	0.3 – 13.7	—

to decline with the onset of the frontal episode. These patterns in wave height and period were likely caused by strong southeasterly winds blowing over a long fetch prior to the second frontal passage, allowing high swell waves to develop. Following the frontal passage, however, strong northerly winds likely generated choppy seas dominated by short, steep waves, whose period gradually increased through non-linear energy transfer as the post-frontal phase progressed.

Water level also appears to have responded to the wind shifts that occurred during the deployment, although with perhaps unexpectedly long lag times (Fig. 5). During both frontal passages, strong southerly winds caused a peak in water level, apparently due to set-up against the adjacent coast. Water level then decreased following the shift to northerly winds that accompanied both post-frontal stages. Unfortunately, the short data record does not permit a detailed discussion of water level responses to frontal passages, which may take place over several days.

Similar to wave height and water level, current velocity also responded noticeably to the prevailing meteorological conditions (Table 3 and Fig. 6). During both frontal passages, current direction was very nearly the same as wind direction for a

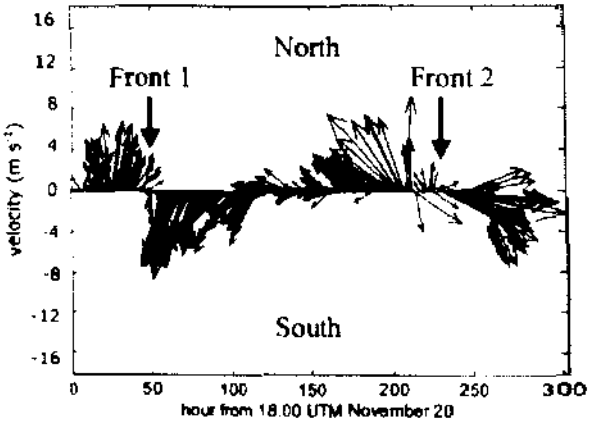

Fig. 3. Hourly wind velocity vectors ($m\ s^{-1}$). Arrows indicate the direction in which the wind was blowing (oceanographic convention).

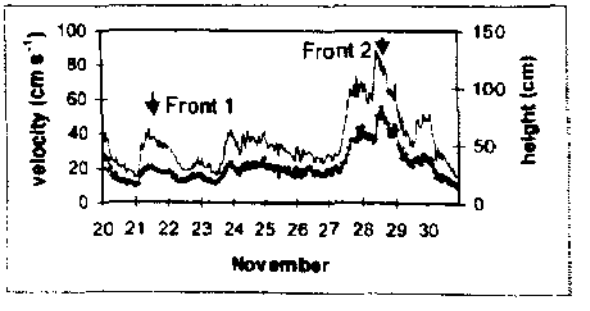

Fig. 4. Significant wave height (smooth line) and wave orbital velocity (marked line) during the study period.

Table 2. Wave characteristics during the deployment. Key: Hs = significant wave height; Tp = peak wave period.

Front	Phase	Hs (m)	Tp (s)	Orbital velocity (cm s^{-1})	Dominant Direction of Propagation
1	Fair	0.36	6.3	15.4	Northeast
	Pre	0.43	5.5	15.9	Northeast
	Front	0.51	5.7	18.4	Northeast
	Post	0.38	5.1	15.8	East
2	Fair	0.54	6.5	21.5	Northeast
	Pre	1.07	7.2	38.2	Northeast
	Front	0.67	7.6	29.5	Northeast
	Post	0.53	5.3	19.9	North
ALL	—	0.52	6.1	21.5	—

significant amount of time and thus rotated clockwise from northward- to southward-flowing as each front passed. The data suggest that currents were driven both by direct wind stress and by "inertial" forces resulting from relaxation of sea level set-up as discussed by Daddio (1977). Currents were strongest during the post-frontal phases of both passages when maximum mean current velocity at 120 cm above the bed reached 22 and 21 cm s^{-1}, respectively. This stands in contrast to orbital velocity, which was at its maximum during pre-frontal stages. The current direction during each of the pre-frontal periods differed between the two frontal passages. In the case of Front 1, post-frontal currents were predominantly southward; whereas during Front 2, currents remained northeasterly for the majority of the post-frontal stage before eventually rotating toward the south. Also of note during this deployment were the strong, steady, southward currents that dominated the second fair weather phase.

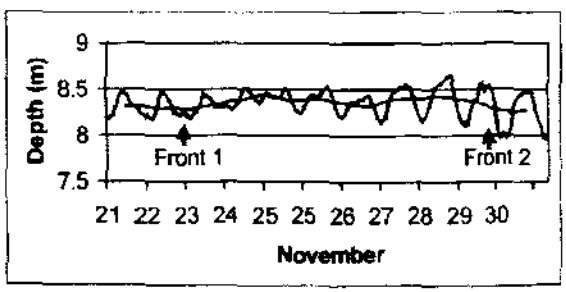

Fig. 5. Hourly water level and water level smoothed using a 24-h moving-average window.

Bottom Boundarty Layer Parameters

Current-induced shear velocity was strong, and logarithmic current profiles were well developed during post-frontal stages (Table 4), which is intuitively consistent with the presence of strong,

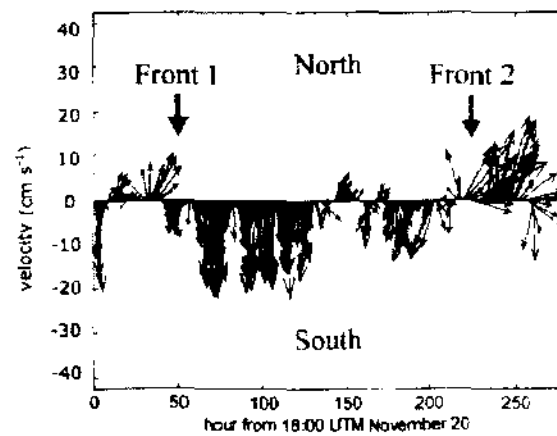

Fig. 6. Mean hourly current velocity vectors (cm s^{-1}) at 120 cm above the bed.

Table 3. Current speed (s) and direction at 20 (bot), 67 (mid), 120 (top) cm above the bed.

Front	Phase	s(top) (cm s^{-1})	s(mid) (cm s^{-1})	s(bot) (cm s^{-1})	Dominant Direction of flow
1	Fair	6.1	5.4	3.2	Variable
	Pre	6.2	5.3	3.4	North
	Front	6.9	5.5	2.3	South
	Post	14.0	12.0	7.3	South
2	Fair	7.5	6.2	3.0	South
	Pre	5.9	5.2	2.6	Variable
	Front	8.8	7.2	3.7	Northeast
	Post	13.4	11.4	6.6	Northeast
ALL	—	9.2	7.8	4.2	—

Table 4. Bottom boundary layer parameters calculated for all hourly bursts with logarithmic profiles. Key: z_{0c} = roughness length; u_{*c} = current shear velocity; u_{*cw} = wave-current shear velocity.

Front	Phase	z_{0c} (cm)	u_{*c} (cm s^{-1})	u_{*cw} (cm s^{-1})	% Logarithmic Profiles
1	Fair	5.0	1.41	2.05	29
	Pre	1.6	0.69	2.23	18
	Front	9.2	1.08	1.87	69
	Post	3.5	1.59	1.94	67
2	Fair	8.2	1.25	2.18	26
	Pre	7.1	0.97	3.08	11
	Front	8.9	1.90	3.08	23
	Post	7.0	1.75	2.10	47
ALL	—	6.1	1.44	2.12	40

steady currents at these times. It is more difficult to make generalizations regarding the combined wave-current shear velocity, because throughout all stages of Front 1, its value remained fairly constant, and low, relative to Front 2. Front 2, in contrast, illustrates the importance of high waves, rather than strong currents, in generating high combined wave-current shear velocities at the study site. Specifically, the highest shear velocities occurred during the pre-frontal and frontal stages, which were characterized by high waves. Shear velocity was low during the post-frontal stage, despite the presence of strong currents. This alone has unclear implications for the net movement of bed sediment within the water column, which requires a combination of entraining forces (shear velocity) and transporting forces (current flow). The sediment transport model accounts for this, however, and the results derived from this model are discussed in the following section.

Table 5. Predicted sediment transport. Key: Q = predicted transport; z<wbl = within the wave boundary layer; z<wbl = above the wave boundary layer; total = throughout the water column. Units are mg cm^{-1} s^{-1}.

Phase	Q (z<wbl)	Direction	Q (z>wbl)	Direction	Q (total)	Direction
1. Fair	7.26	122	1.48	175	8.25	270
Pre	1.23	313	0.21	324	1.43	348
Front	0.27	148	0.086	9	0.39	357
Post	5.17	126	1.65	175	6.39	269
2. Fair	2.23	119	0.19	150	2.40	276
Pre	11.90	120	1.11	168	12.67	168
Front	14.67	110	1.88	69	16.15	146
Post	7.4	357	2.57	49	9.20	142
Average	3.29	104	0.73	140	3.91	110

Sediment Transport

Fronts 1 and 2 differed considerably in terms of both sediment transport magnitude and direction (Table 5). Perhaps the most notable aspect of these results is the high transport rate associated with the pre-frontal and frontal stages of Front 2. Although the transport direction during these time periods is toward the southeast (essentially offshore), it is interesting to note that the transport during the prefrontal and frontal stages of Front 1 is roughly in the opposite direction. Since wave stresses are essentially bi-directional, it is possible that sediment transport direction during cold front passages is very sensitive to the specific meteorological characteristics of the front and the associated current direction, which serve to shift transport toward one component of the wave orbital flow. Furthermore, the majority of predicted transport occurred within the wave boundary layer during all stages, reflecting both the importance of waves in mobilizing sediment in this low-energy environment and the fact that sediment does not likely diffuse very high into the water column. Finally, our predictions indicate that fair weather periods are characterized by low rates of westward sediment transport.

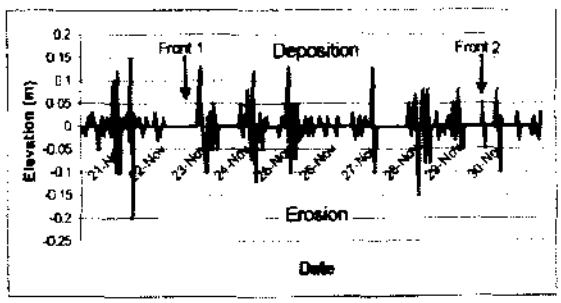

Fig. 7. Bed elevation (m) during the study. The mean bed elevation for the study period has been assigned a value of zero, negative values indicate bed erosion, and positive values indicate bed accretion.

Results from the sonar altimeter (Fig. 7) indicate appreciable movement of bed material throughout the study, including bed height fluctuations of up to 20 cm. These changes occurred over time-scales of hours and included alternating episodes of erosion and deposition, with the result that no net change occurred during the study period. The most logical interpretation for these fluctuations is that bed forms, such as sand ripples, were migrating beneath the altimeter throughout most of the deployment. The time series suggests no particular periodicity to these migrations, which should be expected, given the changing wave and current conditions that occurred. There is also no indication that rates of change were higher during frontal passages than during low energy conditions. There are several possible explanations for this. First, the 30-minute sampling frequency of the

altimeter would not have permitted bed form migration rates greater than one wavelength h^{-1} (as may have occurred during high-energy conditions) to be resolved. Second, rapid changes in the direction of wave and current stresses that accompanied the frontal passages may not have facilitated unidirectional bed form migration, even over a very short time scale. Finally, the increased importance of sediment entrainment and transport high in the water column may have obscured the effects of bed form movement during high-energy conditions. Nevertheless, these measurements are direct field evidence that bed stresses capable of moving sediment were operative during much of the deployment period.

Conclusions

1. High waves and wave-current shear velocities accompanied prefrontal and frontal stages of the cold front passages, facilitating potentially large sediment transport volumes within the wave boundary layer. Transport direction may, however, vary widely.
2. Strong, consistent, currents with highly logarithmic profiles tended to develop following frontal passages. Results do not suggest high sediment transport rates during these periods, however, likely owing to fairly low wave activity.
3. Fair weather periods were characterized by low predicted rates of sediment transport to the west.

Thus, although many researchers have characterized the Louisiana coast as one of low oceanographic energy where transport and deposition of sedimentary material is dominated by fluvial influences, this research indicates that winter cold front passages may generate waves and currents on the Louisiana inner shelf that are powerful enough to resuspend and transport sediment. The direction and magnitude of this transport, however, require further quantification.

ACKNOWLEDGMENTS

We acknowledge the Louisiana State University Coastal Studies Institute Field Support Group for their significant contributions to the design, construction, and deployment of the instrumentation. This work was funded by the Minerals Management Service under contract # 3066/#19911.

LITERATURE CITED

Adams, C. E., Jr., D. J .P. Swift, and J. M. Coleman. 1987. Bottom currents and fluviomarine sedimentation on the Mississippi prodelta shelf: February-May 1984. *Journal of Geophysical Research* 92:14,595-14,609.

Cacchione, D. A., D. E. Drake, J. T. Ferreira, and G. B. Tate. 1994. Bottom stress estimates and sand transport on northern California inner continental shelf. *Continental Shelf Research* 14:1273-1289.

Crout, R. L. and R. D. Hamiter. 1981. Response of bottom waters on the West Louisiana Shelf to transient wind events and resulting sediment transport. *Transactions-Gulf Coast Association of Geological Societies* 31:273-278.

Daddio, E. 1977. Response of coastal waters to atmospheric frontal passage in the Mississippi Delta region. Technical Report No. 234. Coastal Studies Institute, Louisiana State University, Baton Rouge.

Dingler, J. R. and T. E. Reiss. 1990. Cold-front driven storm erosion and overwash in the central part of the Isles Dernieres, a Louisiana barrier-island arc. *Marine Geology* 91:195-206.

Drake, D.E. and D. A. Cacchione. 1992. Wave-current interaction in the bottom boundary layer during storm and non-storm conditions: observations and model predictions. *Continental Shelf Research*12:1331-1352.

Earle, M. D., D. McGehee, and M. Tubman. 1995. Field wave gaging program, wave data analysis standard. Instruction Report CERC-95-1. USACE Waterways Experiment Station, Vicksburg, Mississippi.

Glenn, S. M. and W. D. Grant. 1987. A suspended sediment stratification correction for combined wave and current flows. *Journal of Geophysical Research* 92:8244-8264.

Grant, W. D., and O. S. Madsen. 1979. Combined Wave and Current Interaction with a Rough

Bottom. *Journal of Geophysical Research* 84:1797-1807.

GRANT, W. D. AND O. S. MADSEN. 1986. The continental-shelf bottom boundary layer. *Annual Review of Fluid Mechanics* 18:265-305.

GROSS, T. F., A. E. ISLEY, AND C. R. SHERWOOD. 1992. Estimation of stress and bed roughness during storms on the Northern California Shelf. *Continental Shelf Research* 12:389-413.

JAFFE, B. E., J. H. LIST AND A. H. SALLENGER, JR. 1997. Massive sediment bypassing on the lower shoreface offshore of a wide tidal inlet—Cat Island Pass, Louisiana. *Marine Geology* 136:131-149.

MURRAY, S. P., N. D. WALKER, AND C. E. ADAMS, JR. 1993. Impacts of winter storms on sediment transport within the Terrebonne Bay Marsh Complex. *Coastlines of the Gulf of Mexico: Proceedings of the ASCE Symposium on Coastal and Ocean Management* 8:56-70.

ROBERTS, H. H., O. K. HUH, S. A. HSU, L. J. ROUSE, JR., AND D. RICKMAN. 1987. Impact of cold-front passages on geomorphic evolution and sediment dynamics of the complex Louisiana coast. *Coastal Sediments '87*: 1950-1963.

STONE, G. W. AND P. WANG. 1999. The importance of cyclogenesis on the short term evolution of Gulf coast barriers. *Transactions-Gulf Coast Association of Geological Societies*. 49:478-486.

WIBERG, P. L., D. E. DRAKE AND D. A. CACCHIONE. 1994. Sediment resuspension and bed armoring during high bottom stress events on the northern California inner continental shelf: Measurements and predictions. *Continental Shelf Research* 14:1191-1219.

WRIGHT, L. D. AND C. A. NITTROUER. 1995. Dispersal of river sediments in coastal seas: Six contrasting cases. *Estuaries* 18:494-508.

WRIGHT, L. D., C. R. SHERWOOD AND R. W. STERNBERG. 1997. Field measurements of fair-weather bottom boundary layer processes and sediment suspension on the Louisiana inner continental shelf. *Marine Geology* 140:329-345.